Original citation:
Hiley, Craig I., Playford, Helen Y., Fisher, Janet M., Felix, Noelia Cortes, Thompsett, David, Kashtiban, Reza J. and Walton, Richard I.. (2018) Pair distribution function analysis of structural disorder by Nb5+ inclusion in Ceria : evidence for enhanced oxygen storage capacity from under-coordinated oxide. Journal of the American Chemical Society.

Permanent WRAP URL:
http://wrap.warwick.ac.uk/98020

Copyright and reuse:
The Warwick Research Archive Portal (WRAP) makes this work by researchers of the University of Warwick available open access under the following conditions. Copyright © and all moral rights to the version of the paper presented here belong to the individual author(s) and/or other copyright owners. To the extent reasonable and practicable the material made available in WRAP has been checked for eligibility before being made available.

Copies of full items can be used for personal research or study, educational, or not-for profit purposes without prior permission or charge. Provided that the authors, title and full bibliographic details are credited, a hyperlink and/or URL is given for the original metadata page and the content is not changed in any way.

Publisher's statement:
"This document is the Accepted Manuscript version of a Published Work that appeared in final form in Journal of the American Chemical Society copyright © American Chemical Society after peer review and technical editing by the publisher.
To access the final edited and published work
http://pubs.acs.org/page/policy/articlesonrequest/index.html ."

A note on versions:
The version presented here may differ from the published version or, version of record, if you wish to cite this item you are advised to consult the publisher's version. Please see the 'permanent WRAP URL above for details on accessing the published version and note that access may require a subscription.

For more information, please contact the WRAP Team at: wrap@warwick.ac.uk

warwick.ac.uk/lib-publications

Pair Distribution Function Analysis of Structural Disorder by Nb^{5+} Inclusion in Ceria: Evidence for Enhanced Oxygen Storage Capacity from Under-Coordinated Oxide

Craig I. Hiley,[†] Helen Y. Playford,[‡] Janet M. Fisher,[§] Noelia Cortes Felix,[§] David Thompsett,[§] Reza J. Kashtiban,[ǁ] Richard I. Walton[†]*

[†]Department of Chemistry, University of Warwick, Coventry, CV4 7AL UK, [‡]STFC ISIS Facility, Rutherford Appleton Laboratory, Oxfordshire, OX11 0QX, UK, [§]Johnson Matthey Technology Centre, Sonning Common, Reading, RG4 9NH, UK, [ǁ]Department of Physics, University of Warwick, Gibbet Hill Road, Coventry, CV4 7AL UK.

Supporting Information Placeholder

ABSTRACT: Partial substitution of Ce^{4+} by Nb^{5+} is possible in CeO_2 by co-inclusion of Na^+ to balance the charge, via hydrothermal synthesis in sodium hydroxide solution. Pair distribution function analysis using reverse Monte Carlo refinement reveals that the small pentavalent substituent resides in irregular coordination positions in an average fluorite lattice, displaced away from the ideal cubic coordination towards four oxygens. This results in under-coordinated oxygen, which explains significantly enhanced oxygen storage capacity of the materials of relevance to redox catalysis used in energy and environmental applications.
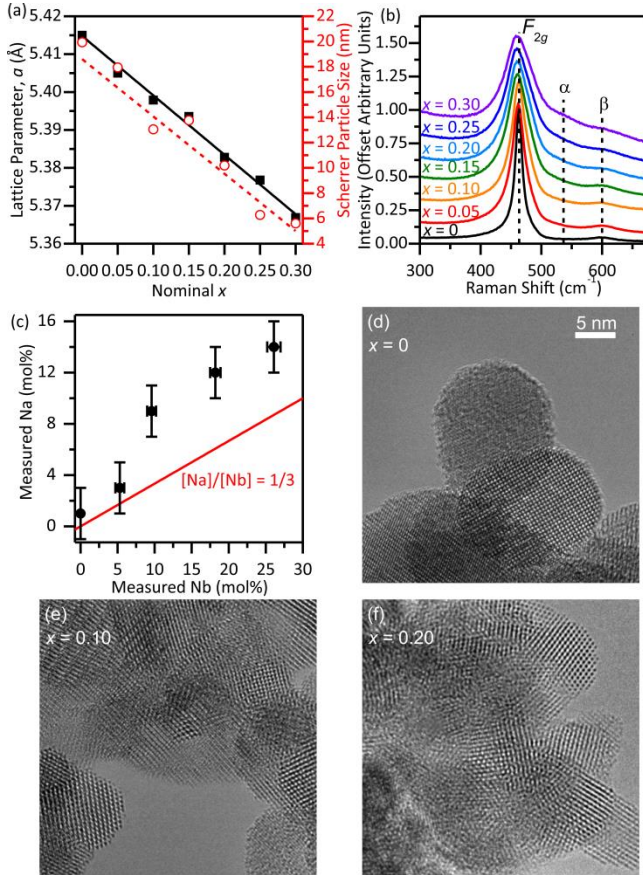
Cerium dioxide, or ceria, has numerous applications in heterogeneous catalysis. The reversible reducibility of Ce^{4+} ions and high mobility of oxide ions in the solid-state[1] give rise to significant oxygen storage properties that make the material an ideal redox-active support for a wide range of catalytic processes such as in automotive emission control,[1b] low temperature water-gas shift catalysis for hydrogen purification[2] and in selective oxidation catalysis for conversion of organics,[3] as well as an oxide-conducting solid-electrolyte.[4] The current focus on ceria-based materials is aimed at further improvement of oxygen storage capacity for new and emerging energy and environmental applications[5] and there is a continued need for new synthetic routes to ceria materials with favorable oxygen storage properties. Inclusion of substituent metals can produce drastic improvements in the redox properties of ceria by introducing strain, increasing the oxide vacancy concentration and/or improving high temperature stability.[6] Many transition-metal cations have been reported as substituents into ceria,[7] and often these are considerably smaller than Ce^{4+} and have a strong preference for octahedral geometry.

In this communication we consider the preparation of substituted ceria by a low-temperature hydrothermal route[8] where the inclusion of the pentavalent niobium leads to thermally robust materials with oxygen storage capacities much greater than pure ceria. The choice of a pentavalent substituent ion is counterintuitive, since its presence alone would imply the need for oxygen excess for charge balance, but we show how Na^+ as co-substituent provides a mechanism for charge balance. Previous work on niobium-containing ceria is limited, compared to the extensive studies made of other substituent cations, but includes materials for catalysis, with rather small amounts of Nb present (typically 5 atom %)[9] or in fact as phase separated oxides,[10] but no structural study has been performed. We use reverse Monte Carlo (RMC) analysis of neutron total scattering data to obtain atomistic structural models for the materials and compare them with unsubstituted ceria: this reveals new information about the extent of oxide-ion disorder in this important class of materials that shows how local structure may be dramatically disrupted by inclusion of substituent cations, despite retaining an average cubic fluorite structure.

Materials were prepared by the hydrothermal reaction of $(1-x)CeCl_3 \cdot 7H_2O$, $xNbCl_5$ and H_2O_2 in NaOH solution at 240 °C (see Supporting Information for full details). For samples with $x \leq 0.30$ all powder XRD peaks from the materials can be indexed to a face-centered fluorite unit cell (Figure S1). When $x = 0$ the refined cell parameter a is 5.415(1) Å, close to the NIST-determined value for highly crystalline CeO_2 (5.411651(1) Å).[11] As x increases, a linear decrease in a is observed to 5.3669(6) Å for $x = 0.30$ (Figure 1a), explained by the inclusion of the smaller Nb into the fluorite lattice. Further to this, the F_{2g} phonon mode in the Raman spectra, associated with eight-coordinate M–O bond vibrations, displays a slight shift to lower wavenumber with increasing x, from 464 cm^{-1} to 459 cm^{-1}, consistent with shorter M–O bonds (Figure 1b);[12] although the effect of decreasing crystal domain size, as observed by Scherrer analysis of powder XRD patterns (Figure 1a) and by HR-TEM (Figure 1d-f)), may also contribute.[13] The intensity of Raman peaks at 540 cm^{-1} and 600 cm^{-1} (labelled α and β, respectively), attributed to second-order phonon modes caused by oxide vacancies/defects,[12-14] increase as a function of x. Ce L_{III}- and Nb K-edge X-ray absorption near-edge structure (XANES) spectra (Figures S3 and S4) give no indication for reduction of the metals from their highest oxidation-states (+4 and +5 for Ce and Nb, respectively). Instead, charge balance in these materials was found to be achieved by adventitious co-substitution of Na from the hydrothermal reaction mixture, to give general formula $(Ce_{1-x}Nb_x)_{1-y}Na_yO_{2-\delta}$ (where $x \leq 0.30$ and $y \geq \sim x/3$). Elemental analysis by ICP-OES shows that the amounts of Na and Nb increase such that the proportion of Na, y, is always at least a third of the Nb content ($\sim x$) (Figure 1c), the

minimum level of Na substitution required to achieve charge balance. The excess Na substituted into the structure allows oxide vacancies, and Na incorporation into complex cerium oxides has been previously shown to generate oxide-deficient fluorite type materi-

als with notably high low-temperature reducibility.[15]

Figure 1. (a) Refined lattice parameter (black) and Scherrer crystallite size (red) from powder XRD of $(Ce_{1-x}Nb_x)_{1-y}Na_yO_{2-\delta}$ as a function of Nb content, x, with lines of best fit. Error bars smaller than data points. (b) Raman spectra with a 514 nm excitation laser. (c) ICP-OES measured Nb and Na content as a percentage of total metal content (remainder Ce). (d-f) HR-TEM micrographs with nominal values of x of 0, 0.10 and 0.20, respectively. All micrographs are presented at the same scale for comparison.

The reducibility of the materials was initially assessed by H_2 temperature-programmed reduction (TPR, Figure 2a), showing that samples exhibit two H_2 uptakes – one at low temperature (<650 °C) and one at higher temperature, widely ascribed to surface and bulk reduction, respectively in ceria itself.[16] The TPR profiles of the substituted materials are very different from the pure CeO_2 material, with a higher onset temperature of reduction, suggesting a different activation mechanism for the redox behavior. Although the bulk reduction remains approximately constant for all values of x, the degree of low temperature reduction increases dramatically as the level of substitution increases, Figure 2b, Table S2 so that ~60% of the Ce^{4+} in the $x = 0.30$ sample is reduced by 650 °C. *In situ* powder XRD under simulated TPR conditions of $(Ce_{0.75}Nb_{0.25})_{1-y}Na_yO_{2-\delta}$ reveals that the average fluorite structure is retained up to at least 800 °C, with a cell parameter increase that far exceeds expected thermal expansion[17] (Figures 2c, S5), and an expanded lattice parameter of 5.4417(1) Å after cooling to room temperature, explained by the reduction of Ce^{4+} to Ce^{3+}, which has a 15-20% larger ionic radius. Subsequent heating in air recovers a fluorite which still has a slightly expanded lattice parameter, possibly due to incomplete re-oxidation, and a second heating cycle in 10% H_2/N_2

again shows a drastic expansion as the Ce^{4+} is again reduced, demonstrating the cyclability of the reduction. Oxygen storage capacity (OSC) measurements were carried out to assess further the kinetically available oxygen in the materials, which is of direct applicability to their use as oxygen buffers in catalytic systems. Alternating pulses of CO and O_2 were passed over a sample (loaded with 0.5 wt% Rh, see Experimental Section) and the breakthrough time (the time taken for CO to be detected in the gas stream after passing over the sample), t, (Figures 2d, S6) of CO was used to calculate the OSC at a given temperature (Figure S7). These data, normalized to surface area to account for morphological effects, demonstrate that OSC per unit area is greatly improved by Nb incorporation (Figure 2e).

The coordination environment of Nb within the fluorite lattice so far remains unclear. Rietveld models in space group $Fm\bar{3}m$ with a mixed metal $4a$ site fail to provide satisfactory agreement with neutron powder diffraction data collected from samples $x = 0.10$, 0.20, 0.30 (Figures S8-11, Table S3). Neutron total scattering data were therefore collected from samples with a nominal composition $x = 0.20$ (both as-made and fired at 500 °C for 5 hours) along with highly crystalline CeO_2 (NIST) and hydrothermally prepared Ce_{1-}
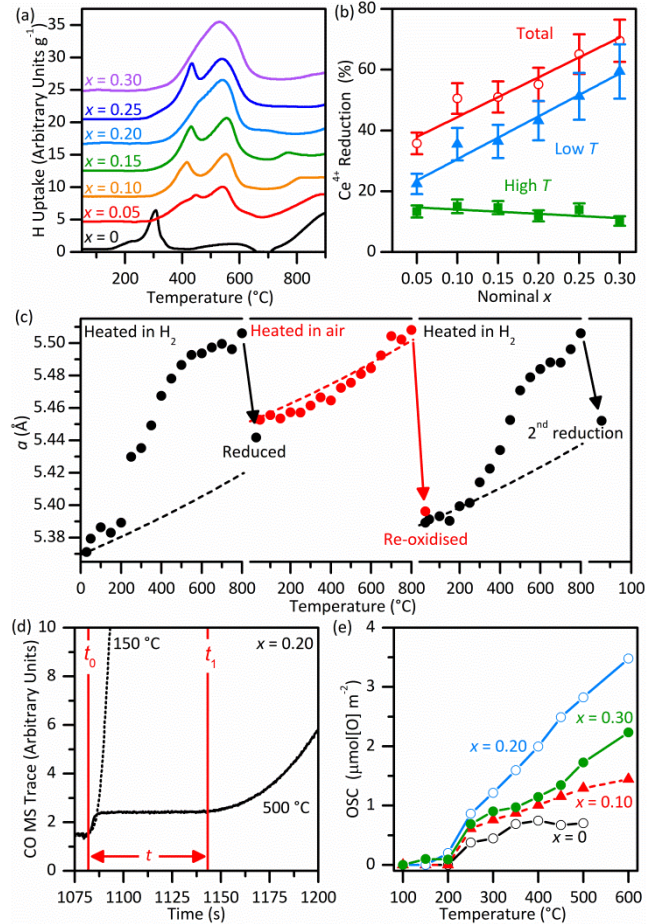

Figure 2. Redox data for $(Ce_{1-x}Nb_x)_{1-y}Na_yO_{2-\delta}$. (a) H_2-TPR profiles normalized to mass of oxide and (b) degree of Ce^{4+} reduction from this H_2 uptake in low (<650 °C) and high (>650 °C) temperature regions, and total Ce reduction as a function of x. (c) Refined lattice parameter of $x = 0.25$ sample as a function of temperature, cycled in 10% H_2/N_2 gas flow (black) and air (red). Dashed lines represent calculated fluorite CeO_2 lattice expansion based on room temperature lattice parameters. (d) Example CO breakthrough measurements at 150 °C and 500 °C for $x = 0.20$, loaded with 0.5 wt% Rh and fired at 500 °C. (e) Calculated OSC per unit area as a function of temperature.

2

$_y$Na$_y$O$_{2-\delta}$ as reference materials. In each case, RMC starting models were generated based on the ideal fluorite structure with composition determined by results from elemental analyses and density measurement (Figure S12). Ce and Na were approximated to a single atom type with a weighted average scattering length because of similarities in both their coordination preference and neutron scattering lengths. Once convergence was reached, the RMC-refined models provide excellent fits to all input datasets, including the PDF (Figure 3a), and show that in both as made and fired $x = 0.20$ samples the (Ce,Na) atoms remain close to the fluorite $4a$ site, whilst the Nb atoms are typically uniaxially displaced towards one face of the MO$_8$ cube (Figures 3b and S15). In all cases the (Ce,Na) atoms are only slightly displaced from the ideal site, by an average of 0.10-0.14 Å, whilst Nb atoms in the as-made material have a mean displacement of 0.34 Å, increasing slightly to 0.38 Å in the fired material (Figure 3c). The O atoms in NIST CeO$_2$ and hydrothermally prepared Ce$_{1-y}$Na$_y$O$_{2-\delta}$ (measured $y = 0.01(2)$) were displaced to a similar degree to the (Ce,Na) atoms, with mean values of 0.12 Å and 0.13 Å, respectively, though the model for the $x = 0.20$ sample had a larger mean displacement of 0.17 Å (Figure 3d). Upon firing, the oxide atoms in this material were found close to their ideal sites, with the mean displacement of 0.13 Å. It is unclear if the perturbed oxide lattice in the as made material is a feature of the small particle size: Scherrer analysis of the XRD pattern of the $x = 0.20$ as-made sample give a crystallite size of ~10 nm (Figure 1a), and a not insignificant quantity of the oxide ions will therefore presumably reside in a likely disordered environment on the particles' surface. Analysis of bond distances resulting from the RMC analysis (Figure 3e) shows that the uniaxial displacement of the Nb atoms results in a 4 long (~2.7 Å) and 4 short (~2.0 Å) Nb–O distances in the most extreme cases (Figure S18), but there are also
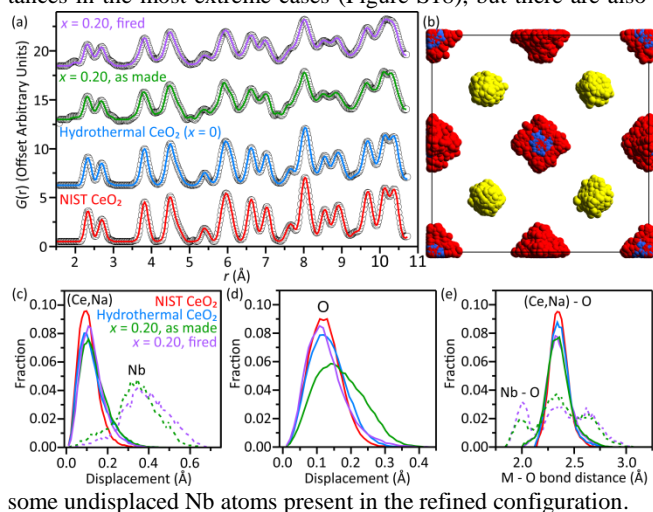
some undisplaced Nb atoms present in the refined configuration.

Figure 3. (a) RMC-fitted radial distribution functions obtained from total neutron scattering data. Data were collected on GEM or Polaris Instruments at ISIS Neutron Spallation Source. (b) $10\times10\times10$ supercell from RMC fit to fired $x = 0.20$ sample collapsed onto a single fluorite unit cell. (Ce,Na) atoms in blue, Nb atoms in red and O atoms in yellow. (c) and (d) Distributions of displacements of each atom type from their 'ideal' sites in each RMC model. (e) Resulting distribution of $M - O$ bond distances in each RMC model.

As a result of the displacement of Nb^{5+} cations from the ideal cubic symmetry, a significant portion of the oxygen atoms become under-coordinated. This can be visualized in Figure 4, where the oxygen lattices from the refined RMC models are shown, colored by their coordination number. Any metal atoms found within 2.5 Å of an oxygen atom were considered to be coordinated to it. This value was chosen as it encompasses the expected M-O distances in CeO$_2$ and in Nb$_2$O$_5$. In Figure 4 it can be seen that the vast majority

of oxygen atoms in NIST ceria have the expected coordination number, whereas in the Nb-substituted samples a large proportion have a coordination number of 3 and 2. The percentages of under-coordinated oxygen are 17%, 23%, 46% and 45% in NIST CeO$_2$, hydrothermal Ce$_{1-y}$Na$_y$O$_{2-\delta}$, fired (Ce$_{1-x}$Nb$_x$)$_{1-y}$Na$_y$O$_{2-\delta}$ and as made
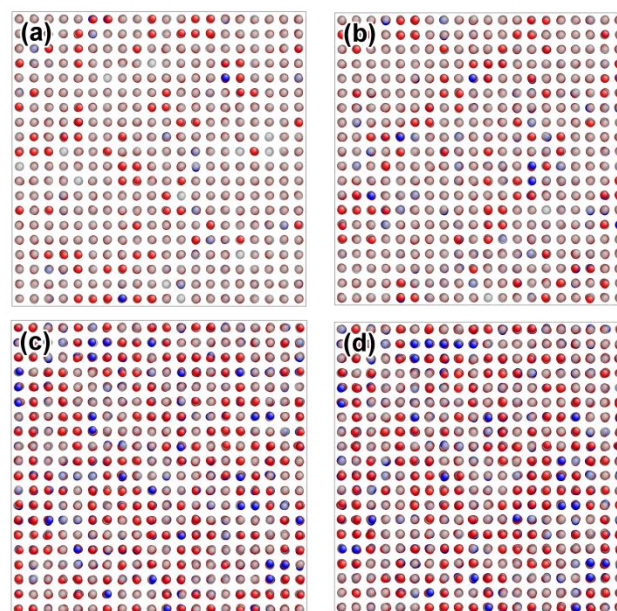

Figure 4. Oxygen atoms from refined RMC configurations, colored by coordination number. Gray, red and blue spheres are 4, 3 and 2-coordinate oxygen, respectively. (a) NIST CeO$_2$, (b) hydrothermal CeO$_2$, (c) fired $x = 0.20$ and (d) as-made $(Ce_{1-x}Nb_x)_{1-y}Na_yO_{2-\delta}$, respectively.

(Ce$_{1-x}$Nb$_x$)$_{1-y}$Na$_y$O$_{2-\delta}$, respectively.

In conclusion, a set of nanocrystalline ceria materials co-substituted with niobium and sodium have been prepared by low-temperature hydrothermal synthesis. RMC analysis of PDF data show that many of the niobium ions are uniaxially displaced from the fluorite metal site in order to achieve four Nb–O bonds of ideal length. After firing at 500 °C, the oxide lattice is ordered, whilst the niobium site remains displaced, leading to under-coordinated oxide ions. The new materials can be compared favorably with the widely studied ceria-zirconia solid solutions, which have significant oxygen storage capacity despite a lack of oxide vacancies;[6b] providing another example of how local structural strain eases oxide mobility and reducibility of an oxide. The counterintuitive substitution of a small pentavalent cation is aided by the coordinative insouiance of Nb^{5+}, allowing its inclusion in the fluorite lattice in highly irregular geometry, leads to under-coordinated oxide that must be responsible for favorable oxygen storage properties.

ASSOCIATED CONTENT

Supporting Information

Detailed experimental procedures and additional characterization data. The Supporting Information is available free of charge on the ACS Publications website. The research data supporting this publication can be accessed at wrap.warwick.ac.uk

AUTHOR INFORMATION

Corresponding Author

*r.i.walton@warwick.ac.uk

ACKNOWLEDGMENT

REFERENCES

(1) (a) *Catalytic Science Series: Volume 12: Catalysis by Ceria and Related Materials, 2nd Edition* Trovarelli, A.; Fornasiero, P., Eds.; Imperial College Press: London, 2012; (b) Montini, T.; Melchionna, M.; Monai, M.; Fornasiero, P. *Chem. Rev.* **2016**, *116*, 5987.

(2) Gorte, R. J.; Zhao, S. *Catal. Today* **2005**, *104*, 18.

(3) (a) Colussi, S.; Gayen, A.; Camellone, M. F.; Boaro, M.; Llorca, J.; Fabris, S.; Trovarelli, A. *Angew. Chem.-Int. Edit.* **2009**, *48*, 8481; (b) Beckers, J.; Rothenberg, G. *Green Chemistry* **2010**, *12*, 939; (c) Cargnello, M.; Delgado Jaen, J. J.; Hernandez Garrido, J. C.; Bakhmutsky, K.; Montini, T.; Calvino Gamez, J. J.; Gorte, R. J.; Fornasiero, P. *Science* **2012**, *337*, 713.

(4) Tuller, H. L.; Nowick, A. S. *J. Electrochem. Soc.* **1975**, *122*, 255.

(5) (a) Bumajdad, A.; Eastoe, J.; Mathew, A. *Adv. Colloid Interface Sci.* **2009**, *147-48*, 56; (b) Chueh, W. C.; Falter, C.; Abbott, M.; Scipio, D.; Furler, P.; Haile, S. M.; Steinfeld, A. *Science* **2010**, *330*, 1797; (c) Valechha, D.; Lokhande, S.; Klementova, M.; Subrt, J.; Rayalu, S.; Labhsetwar, N. *J. Mater. Chem.* **2011**, *21*, 3718; (d) Sun, C.; Li, H.; Chen, L. *Energy Environ. Sci.* **2012**, *5*, 8475; (e) Walkey, C.; Das, S.; Seal, S.; Erlichman, J.; Heckman, K.; Ghibelli, L.; Traversa, E.; McGinnis, J. F.; Self, W. T. *Environmental Science-Nano* **2015**, *2*, 33.

(6) (a) Park, S.; Vohs, J. M.; Gorte, R. J. *Nature* **2000**, *404*, 265; (b) Di Monte, R.; Kaspar, J. *J. Mater. Chem.* **2005**, *15*, 633.

(7) Hiley, C. I.; Walton, R. I. *CrystEngComm* **2016**, *18*, 7656.

(8) Walton, R. I. *Prog. Cryst. Growth Charact. Mater.* **2011**, *57*, 93.

(9) (a) Ramirez-Cabrera, E.; Atkinson, A.; Chadwick, D. *Appl. Catal. B-Environ.* **2002**, *36*, 193; (b) Ramirez-Cabrera, E.; Laosiripojana, N.; Atkinson, A.; Chadwick, D. *Catal. Today* **2003**, *78*, 433; (c) Qu, R.; Gao, X.; Cen, K.; Li, J. *Appl. Catal. B* **2013**, *142*, 290.

(10) Casapu, M.; Bernhard, A.; Peitz, D.; Mehring, M.; Elsener, M.; Kroecher, O. *Appl. Catal. B-Environ.* **2011**, *103*, 79.

(11) *SRM 674b; X-Ray Powder Diffraction Intensity Set* National Institute of Standards and Technology; US Department of Commerce Gaithersburg, MD (2012)

(12) Li, L.; Chen, F.; Lu, J. Q.; Luo, M. F. *J. Phys. Chem. A* **2011**, *115*, 7972.

(13) Spanier, J. E.; Robinson, R. D.; Zhang, F.; Chan, S.-W.; Herman, I. P. *Phys. Rev. B* **2001**, *64*, 245407.

(14) Fernández-García, M.; Martínez-Arias, A.; Hanson, J. C.; Rodriguez, J. A. *Chem. Rev.* **2004**, *104*, 4063.

(15) Wright, C. S.; Walton, R. I.; Thompsett, D.; Fisher, J.; Ashbrook, S. E. *Adv. Mater.* **2007**, *19*, 4500.

(16) (a) Perrichon, V.; Laachir, A.; Bergeret, G.; Frety, R.; Tournayan, L.; Touret, O. *J. Chem. Soc., Faraday Trans.* **1994**, *90*, 773; (b) Ranga Rao, G. *Bull. Mater. Sci.* **1999**, *22*, 89; (c) Giordano, F.; Trovarelli, A.; de Leitenburg, C.; Giona, M. *J. Catal.* **2000**, *193*, 273; (d) Ranga Rao, G.; Mishra, B. G. *Bull. Catal. Soc. India* **2003**, *2*, 122.

(17) Taylor, D. *Trans. J. Brit. Ceram. Soc.* **1984**, *83*, 32.

For Table of Contents Only

$(Ce_{1-x}Nb_x)_{1-y}Na_yO_{2-\delta}$